Coherence Properties of Shallow Donor Qubits in ZnO

Xiayu Linpeng, Maria L.K. Viitaniemi, Aswin Vishnuradhan, Y. Kozuka, Cameron Johnson, M. Kawasaki, and Kai-Mei C. Fu

Phys. Rev. Applied **10**, 064061 — Published 28 December 2018

DOI: 10.1103/PhysRevApplied.10.064061

Coherence properties of shallow donor qubits in ZnO

Xiayu Linpeng,[1,*] Maria L. K. Viitaniemi,[1] Aswin Vishnuradhan,[2] Y. Kozuka,[2,3] Cameron Johnson,[4] M. Kawasaki,[2] and Kai-Mei C. Fu[1,5,†]

[1] *Department of Physics, University of Washington, Seattle, Washington 98195, USA*
[2] *Department of Applied Physics and Quantum-Phase Electronics Center (QPEC), University of Tokyo, Tokyo 113-8656, Japan*
[3] *JST, PRESTO, Kawaguchi, Saitama 332-0012, Japan*
[4] *Department of Physics, University of Oregon, Eugene, Oregon 97403, USA*
[5] *Department of Electrical Engineering, University of Washington, Seattle, Washington 98195, USA*

(Dated: November 28, 2018)

Defects in crystals are leading candidates for photon-based quantum technologies, but progress in developing practical devices critically depends on improving defect optical and spin properties. Motivated by this need, we study a new defect qubit candidate, the shallow donor in ZnO. We demonstrate all-optical control of the electron spin state of the donor qubits and measure the spin coherence properties. We find a longitudinal relaxation time T_1 exceeding 100 ms, an inhomogeneous dephasing time T_2^* of 17 ± 2 ns, and a Hahn spin-echo time T_2 of 50 ± 13 µs. The magnitude of T_2^* is consistent with the inhomogeneity of the nuclear hyperfine field in natural ZnO. Possible mechanisms limiting T_2 include instantaneous diffusion and nuclear spin diffusion (spectral diffusion). These dephasing mechanisms suggest that with isotope and chemical purification qubit coherence times can be extended. This work motivates further research on high-purity material growth, quantum device fabrication, and high-fidelity control of the donor:ZnO system for quantum technologies.

I. INTRODUCTION

Defect centers in crystals have attracted significant attention as qubit candidates for quantum communication [1, 2] and computation [3] due to the ability to realize spin-photon entanglement and scalable device integration. A two-node network, the fundamental building block for measurement-based quantum computation [4–6] and long-range quantum communication [7, 8], can be generated via a single photon measurement on two non-interacting, spatially separated qubits. The quantum link efficiency, i.e. the ratio between the entanglement generation and the decoherence rates, determines the scalability of a network. Finding a system which combines homogeneous and efficient optical properties with a long spin coherence time is still an outstanding challenge. The negatively charged nitrogen-vacancy (NV) center [9, 10] in diamond is one of the leading candidates for the photon based protocols and two-node networks have been demonstrated [11]. However, the entanglement generation rate is typically low, limited by nonideal optical properties such as optical inhomogeneity, spectral diffusion, and low zero-phonon radiative efficiency. Whilst numerous efforts are focused on overcoming these challenges in diamond [12] and related SiC systems [13, 14], searching for new defect centers with better properties is an alternative solution. Donors in isotope purified ^{28}Si have shown promising features such as ultra-long coherence times [15, 16] and high fidelity qubit control [17]. However, the indirect band gap of Si makes photon-mediated entanglement and therefore the development of scalable quantum networks challenging [4, 18, 19]. While there are photon emitting defects in Si [20–22], the radiative efficiency is typically low. Studies of defect systems in direct band-gap III-V materials, such as quantum dots and donors, have demonstrated efficient optical transitions, spin control and spin readout [23–27]. A two-node network with a kHz generation rate has been realized in the positively-charged quantum dot system [28]. However, due to the lack of a spin-free host matrix, the spin coherence times in III-V systems are limited by hyperfine interactions with the host nuclear spins [28, 29]. Donors in direct band-gap II-VI semiconductors similarly boast efficient optical transitions [30] and, as we show here in ZnO, can exhibit long coherence times. Critical for long-term qubit viability is the compatibility of ZnO with microfabrication processing [31, 32] and the possibility of entanglement generation between the ZnO donor electron and donor/lattice nuclei based on the hyperfine interaction [33]. This electron-nucleus register, demonstrated in both P:Si [34] and NV:diamond systems [35], enables deterministic network scaling in the presence of large photon loss [4, 36].

In this paper, we measure the relaxation and coherence properties of an ensemble of Ga donors in ZnO. Ensemble spin initialization is demonstrated using resonant continuous-wave (cw) excitation. The longitudinal spin relaxation time T_1 shows a $B^{-3.5}$ relationship, dominated by a spin-orbit mediated phonon interaction. The longest T_1 observed in the experiment is ∼0.1 s at 2.25 T, with T_1 increasing with decreasing field. Coherent spin control of donor electrons is achieved with ultra fast optical pulses, red-detuned from the neutral donor (D^0) to donor-bound exciton (D^0X) resonance. The D^0 coherence is then probed via all-optical Ramsey interferometry and spin-echo measurements [25]. The inhomogeneous dephasing time T_2^* is measured to be 17 ± 2 ns which is consistent with the theoretical estimates of inhomogeneous electron-nuclear hyperfine interaction in natural ZnO. The effect of the inhomogeneous nuclear field is suppressed by a spin echo sequence with a measured spin-echo time T_2 of 50 ± 13 µs at 5 T. Possible mechanisms limiting T_2 include spectral diffusion

* lpxy1992@uw.edu
† kaimeifu@uw.edu

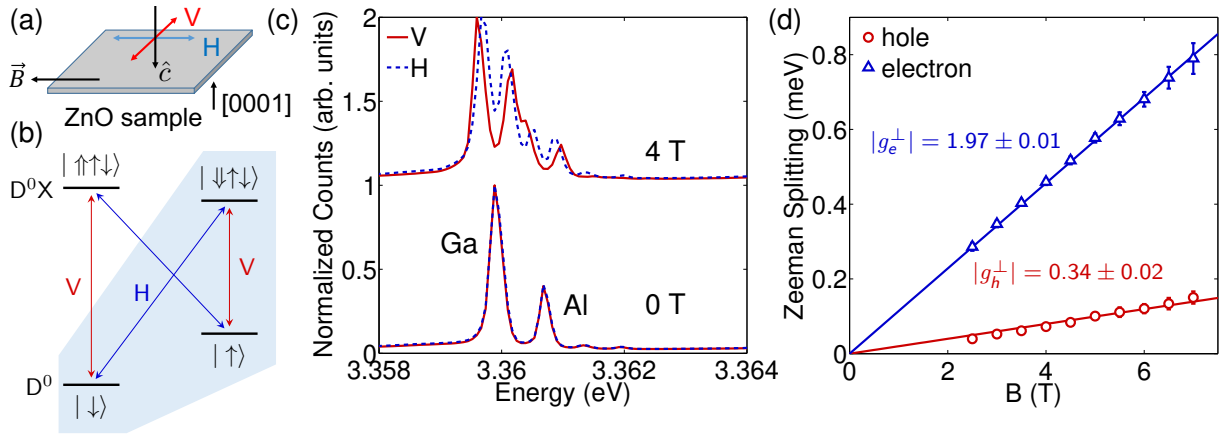

FIG. 1: (a) Experimental geometry. $\hat{c}$ is the optical propagation axis. $\vec{B}$ is the magnetic field. V and H represent vertical polarization ($\hat{\varepsilon} \perp \vec{B}$) and horizontal polarization ($\hat{\varepsilon} \parallel \vec{B}$), respectively. (b) Energy diagram of the donor system at magnetic field in the Voigt geometry. $|\Uparrow\rangle(|\uparrow\rangle)$ denotes the hole (electron) spin. The shaded area shows the Λ system used for the spin initialization and readout. (c) Spectra at 0 T and 4 T with V and H polarized collection. The excitation laser is at 3.446 eV with vertical polarization. Temperature is 5.5 K. Both the Ga and Al donor peaks split into 4 different peaks with applied magnetic field. (d) Electron and hole Zeeman splitting of the Ga donor as function of magnetic fields. The red and blue lines are linear fits of the Zeeman splitting. For these data, both the excitation and collection spot sizes are ∼1 µm.

due to flip-flops of ^{67}Zn nuclear spin pairs [37] and instantaneous diffusion due to the rephasing pulse in the spin echo sequence [38].

II. SETUP AND PHOTOLUMINESCENCE SPECTRUM

The ZnO sample studied in this paper is a 360 µm thick Tokyo Denpa ZnO crystal. The sample included a 0.7 µm high-purity ZnO epilayer grown by molecular beam epitaxy [39], however the measurement signal was dominated by substrate donor emission. The total donor concentration is on the order 10^{17} cm^{-3}, determined by capacitance-voltage measurements [40]. The sample is mounted in a continuous flow cryostat with a superconducting magnet in Voigt geometry, i.e. $\hat{c} \perp \vec{B}$, where $\hat{c}$ is the optical propagation axis, as shown in Fig. 1(a). $\hat{c}$ is parallel to the [0001] direction of the ZnO crystal. All measurements are performed at temperatures between 1.5 and 5.5 K.

The energy diagram of the shallow donor in a magnetic field is shown in Fig. 1(b). The D^0 spin states split due to the electron Zeeman effect. The Zeeman splitting of the D^{0}X state is solely determined by the hole spin, as the two bound electrons form a spin singlet. The two ground spin states $|\uparrow\rangle$, $|\downarrow\rangle$ and the excited state $|\Downarrow\uparrow\downarrow\rangle$ form the Λ system which is used for spin initialization and readout. Typical spectra at 0 T and 4 T are shown in Fig. 1(c). At 0 T, the two main peaks correspond to Al donors (3.3607 eV) and Ga donors (3.3599 eV) [41]. To further confirm the two peaks are from donors, PL spectra with resonant excitation are taken to demonstrate the correlation between the main donor peaks and the corresponding two electron satellite transitions [42], i.e. transitions from the D^{0}X to the 2s and 2p D^0 orbital states. At 4 T, the Al and Ga peaks each split into 4 peaks due to the electron and hole Zeeman splitting. The polarization dependence of the 4 peaks confirms the Γ_7 valence band symmetry assignment [43]. The measured in-plane g-factors for the Ga donors are $|g_e^\perp| = 1.97 \pm 0.01$ and $|g_h^\perp| = 0.34 \pm 0.02$, determined by linear fits of the electron and hole Zeeman splitting at different fields, as shown in Fig 1(d). For the remainder of the paper, we will focus on the Ga donor.

D^{0}X centers (Al, Ga and In) in ZnO exhibit short radiative lifetimes of ∼1 ns [30] and Huang-Rhys parameters <0.1 [30] which indicate high radiative efficiency in the zero-phonon line. This provides a natural Λ system for Raman-based photon-heralded entanglement schemes [44]. The ability to utilize other valence-band D^{0}X transitions [41, 45, 46] to realize highly desirable cycling transitions and "L"-shaped systems will be investigated in future work.

III. SPIN INITIALIZATION AND T_1 MEASUREMENT

Spin initialization, the first step to utilize the spin as a qubit, is performed by optical pumping. A cw pump pulse is resonantly applied on either the $|\uparrow\rangle \Leftrightarrow |\Downarrow\uparrow\downarrow\rangle$ or $|\downarrow\rangle \Leftrightarrow |\Downarrow\uparrow\downarrow\rangle$ transition to initialize to $|\downarrow\rangle$ or $|\uparrow\rangle$, respectively. To visualize the optical pumping, the spins are first prepared using a scrambling pulse, i.e. a series of high power laser pulses with photon energy higher than the donor transitions. Then a cw pump pulse is applied resonantly on the $|\uparrow\rangle \Leftrightarrow |\Downarrow\uparrow\downarrow\rangle$ transition to initialize to $|\downarrow\rangle$. PL from the $|\downarrow\rangle \Leftrightarrow |\Downarrow\uparrow\downarrow\rangle$ transition is collected during the pump pulse. A typical optical pumping curve is shown in Fig. 2(a). An estimate of the pumping efficiency using the contrast ratio of the optical pumping curve [35] yields a fidelity of 95% at

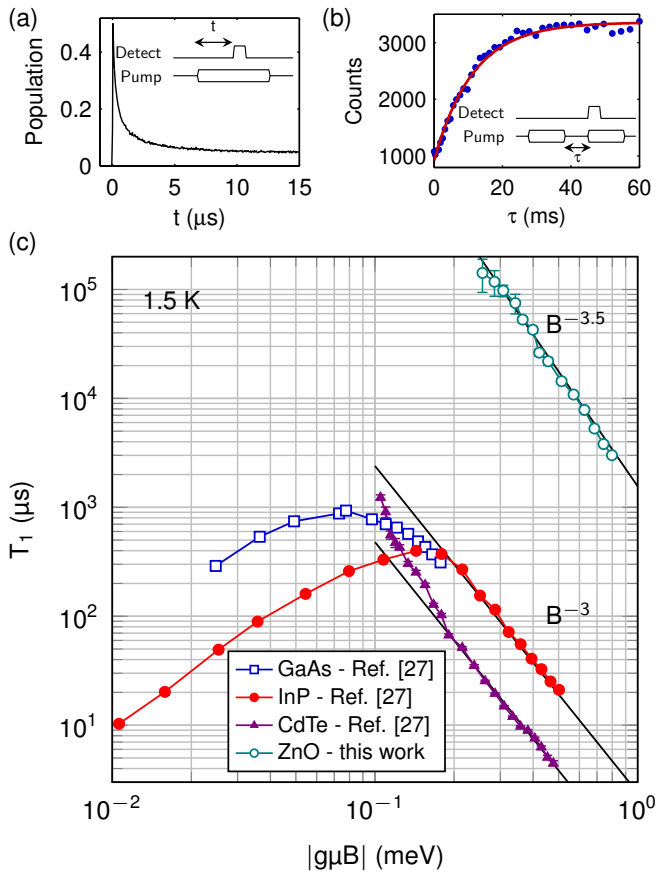

FIG. 2: (a) Optical pumping curve at 5 T, 1.5 K. The inset shows the laser sequence. The PL is detected by an avalanche photodiode with a 50 ns timing resolution. (b) The population recovery curve at 5 T, 1.5 K. The inset shows the corresponding laser sequence. The exponential fit of the recovery curve gives $T_1 = 11.4 \pm 0.5$ ms. (c) The longitudinal spin relaxation time T_1 as a function of the Zeeman energy for donors in GaAs, InP, CdTe and ZnO. The data for GaAs, InP and CdTe is reproduced from a prior work [47]. For the ZnO data, both the excitation and collection spot sizes are ∼1 μm.

1.5 K and 5 T. This estimate assumes that the scrambling pulse prepares the spins with equal population in $|\uparrow\rangle$ and $|\downarrow\rangle$. The efficiency of the optical pumping decreases with decreasing magnetic field. At low field, the Zeeman energy becomes comparable to the optical linewidth of the D^0X transitions. In this case, population in $|\downarrow\rangle$ can be simultaneously pumped back to $|\uparrow\rangle$. For this reason, we are only able to observe an optical pumping signal at fields larger than 2.25 T.

T_1 is measured by recording the population recovery to thermal equilibrium after spin initialization. The spin is initialized to $|\uparrow\rangle$ using a 50 μs cw pulse on resonance with the $|\downarrow\rangle \Leftrightarrow |\Downarrow\uparrow\downarrow\rangle$ transition. Then after waiting for a variable time τ, another 50 μs cw pulse is applied and the PL of the $|\uparrow\rangle \Leftrightarrow |\Downarrow\uparrow\downarrow\rangle$ transition is collected in the first 1 μs window of the cw pulse. The collected PL signal is proportional to the $|\downarrow\rangle$ population. By changing τ, a population recovery curve is measured and T_1 is extracted using an exponential fit (Fig. 2(b)).

T_1 at 1.5 K as function of magnetic field is shown in Fig. 2(c), with previous measurement results in GaAs, InP and CdTe [47] included for comparison. In the high-field region, the strong inverse power dependence on B indicates that relaxation is induced by phonon interactions, mediated by electron spin-orbit coupling [48]. The high B-field dependence in ZnO is similar to what is observed in the other three semiconductors. However, $T_{1,\mathrm{ZnO}}$ is over two orders of magnitude longer as a result of lower spin-orbit coupling. The longest observed T_1 is 0.14 ± 0.05 s at 2.25 T. This is 10^5 times longer than previously reported results in ZnO epilayers [45].

At low field, a positive B-field dependence of T_1 is observed in GaAs and InP due to the inhomogeneous static hyperfine field and the short electron correlation time at the donor sites [47]. In ZnO, this mechanism is expected to be weaker because of the small electron Bohr radius and thus longer correlation time. The high B-field dependence, together with the small Bohr radius, suggest T_1 can approach and possibly exceed seconds at lower magnetic fields. Control of the spin at lower fields will require a high-purity sample with narrow optical linewidth, as optical pumping can only be efficient if the linewidth is much smaller than the Zeeman splitting.

IV. OPTICAL SPIN COHERENT CONTROL

In the next series of measurements we use ultrafast optical pulses to create and probe the electron spin coherence. To obtain both strong optical pumping efficiency and long T_1, we choose an intermediate magnetic field to study, i.e. 5 T. At 5 T, the large electron Zeeman splitting (138 GHz) makes direct microwave control of the electron spin challenging. An alternative is to use a detuned ultra-fast optical pulse to coherently rotate the spins [26, 49], which can be understood using a 4-level density matrix model. For the 4-level donor system, the Hamiltonian in the interaction picture with the rotating wave approximation is

$$H = \begin{pmatrix} 0 & 0 & -\frac{\Omega_{13}(t)}{2} & -\frac{\Omega_{14}(t)}{2} \\ 0 & \omega_e & -\frac{\Omega_{23}(t)}{2} & -\frac{\Omega_{24}(t)}{2} \\ -\frac{\Omega^*_{13}(t)}{2} & -\frac{\Omega^*_{23}(t)}{2} & \Delta & 0 \\ -\frac{\Omega^*_{14}(t)}{2} & -\frac{\Omega^*_{24}(t)}{2} & 0 & \Delta + \omega_h \end{pmatrix}, \quad (1)$$

where $\omega_e(\omega_h)$ is the energy of the electron (hole) Zeeman splitting, Δ is the red detuning between the ultra-fast laser and the transition $|\downarrow\rangle \Leftrightarrow |\Downarrow\uparrow\downarrow\rangle$, $\Omega_{ij}(t) = \overrightarrow{\mu_{ij}} \cdot \overrightarrow{E}(t)/\hbar$ is the product of the electric field and the dipole matrix element of transition $|i\rangle \Leftrightarrow |j\rangle$ ($i = 1, 2, 3, 4$ corresponding to states $|\downarrow\rangle$, $|\uparrow\rangle$, $|\Downarrow\uparrow\downarrow\rangle$, $|\Uparrow\uparrow\downarrow\rangle$). In the far-detuned limit ($\Delta \gg$ the optical pulse width), the populations of the two excited states can be adiabatically eliminated [50] and Eq. 1 reduces to an effective 2-level Hamiltonian describing coherent rotations of the electron spin.

In our experiment, the polarization of the laser is adjusted

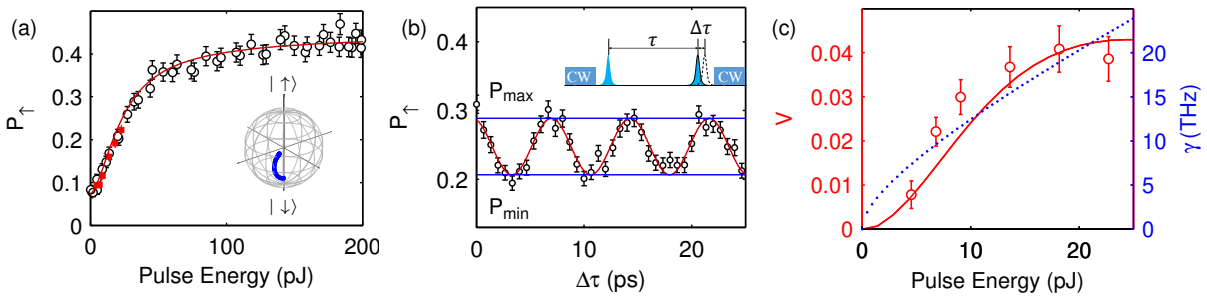

FIG. 3: (a) $P_\uparrow$ (population of $|\uparrow\rangle$) as a function of the single-pulse energy with spin initialized to $|\downarrow\rangle$ and then excited by the ultra-fast pulse. Error bars show the 1σ uncertainty from the Poisson noise in PL collection. Data points represented by red squares at low powers are taken at the same power as data points in **c**. The red curve is a simultaneous least squares fit for data in **a** and **c**. The inset shows how the state changes in the Bloch sphere using the simulated results. (b) A typical Ramsey interference pattern with 18 pJ pulse energy. The inset shows the laser sequence, where τ is the delay between the two pulses ($\tau = 0.8$ ns in this data). The first cw pulse initializes the spin and the second cw pulse is to used to read out. (c) The Ramsey fringe amplitude V = (P_{max} - P_{min})/2 as a function of the single pulse energy. Error bars show the 1σ uncertainty from the sinusoid fit of the Ramsey oscillation. The red line is the simulation result from the simultaneous fit. The blue dotted line shows the fit parameter γ (excited state dephasing rate) as a function of pulse energy. For these data, the excitation spot size is ∼2 μm, the collection spot size is ∼0.6 μm. The temperature is at 1.5 K and the magnetic field is at 5 T. The ultra-fast pulses are detuned by $\Delta/2\pi = 3.57$ THz from the transition $|\downarrow\rangle \Leftrightarrow |\Downarrow\uparrow\downarrow\rangle$.

so that $\Omega_{13} = \Omega_{23} = \Omega_{14} = \Omega_{24} = \Omega_R$ [42]. The ZnO donor effective Hamilitonian is then given by [42]

$$H_{\text{eff}} = \begin{pmatrix} 0 & \frac{\Omega_{\text{eff}}(t)}{2} e^{-i\omega_e t} \\ \frac{\Omega^*_{\text{eff}}(t)}{2} e^{i\omega_e t} & 0 \end{pmatrix}, \qquad (2)$$

where $\Omega_{\text{eff}} = \frac{|\Omega_R|^2}{2}(\frac{1}{\Delta} + \frac{1}{\Delta+\omega_h})$ is the effective Rabi frequency. The axis of the rotation is determined by the timing of the pulse due to the $e^{\pm i\omega_e t}$ terms in H_{eff}. While this 2-level model provides intuition for how a single optical pulse coherently rotates the spin, it does not consider decoherence or relaxation. To analyze the dynamics of the density matrix in a more accurate way, we use the full 4-level master equation with decoherence and relaxation taken into consideration, i.e. $\partial\rho/\partial t = -i[H, \rho] + L(\rho)$, where $L(\rho)$ is the Lindblad operator [42]. All data in Fig. 3 is fit using this 4-level master equation model.

To generate a coherent superposition of the ground spin states, we first optically pump the donors to $|\downarrow\rangle$. We next apply an ultra-fast control pulse obtained by frequency doubling an 1.9 ps pulse generated from a mode-locked Ti:Sapphire laser. The population $P_\uparrow$ is measured by the subsequence cw pumping pulse [42]. Figure 3(a) shows the dependence of $|\uparrow\rangle$ population after the ultrafast pulse as a function of the pulse energy. We attribute the saturation of the population transfer at high pulse powers to laser-induced dephasing between the D^0X states and the D^0 states. At high power, the coherence between the excited states and the ground states decays much faster than the pulse duration. In this high power regime, the ultra-fast pulse can no longer coherently drive the transition between the two spin states and a saturation in the population curve is observed. While the mechanism for this dephasing is unknown, one possibility is the unintentional excitation of real carriers.

Due to the laser-induced dephasing, coherent rotations are only expected at low pulse energy. The coherence of the small-angle rotation can be probed via Ramsey interferometry. Standard Ramsey experiments are done by measuring the spin population after two $\pi/2$ pulses with variable delay between them. An oscillation of the spin population as a function of the delay time can be observed due to the Larmor precession of the electron spin. Though only small-angle rotations are accessible in our system, they can also produce Ramsey interference, albeit with smaller oscillation amplitude. A representative Ramsey fringe using small-angle rotations is shown in Fig. 3(b). The fit oscillation frequency in Fig. 3(b) is 136 ± 3 GHz at 5 T, which matches the predicted 137.9 ± 0.7 GHz using the measured electron g-factor. The Ramsey fringe amplitude as a function of the pulse energy is shown in Fig. 3(c). A least squares fit based on the 4-level density matrix model is used to fit the data in Fig. 3(a) and (c) simultaneously. An empirical relationship between $\Omega_R(t)$ and the laser-induced dephasing rate γ is used in the fit, i.e. $\gamma = \beta_1\Omega_R(t) + \beta_2\Omega_R^2(t)$, where $\beta_{1,2}$ are the fitting parameters. The other fit parameter is α which relates the optical Rabi frequency $\Omega_R(t)$ and physical pulse energy $P = \alpha \cdot \max|\Omega_R(t)|^2$.

Ultra-fast optical spin-control is a powerful tool to probe the coherence of the electron spins and measure the coherence time, however long-term it will be necessary to achieve high fidelity full-angle control for quantum applications. A possible solution is to utilize spin-resonant microwave fields, which has been successfully demonstrated in NV centers and donors in Si. For practical devices in ZnO, we must decrease our magnetic field such that the electron Zeeman splitting of the ground states is less than 10 GHz. This is difficult in our current sample due to the large inhomogeneous optical linewidth which makes optical pumping inefficient at lower magnetic fields. This challenge can be overcome with higher

purity samples or single donor isolation.

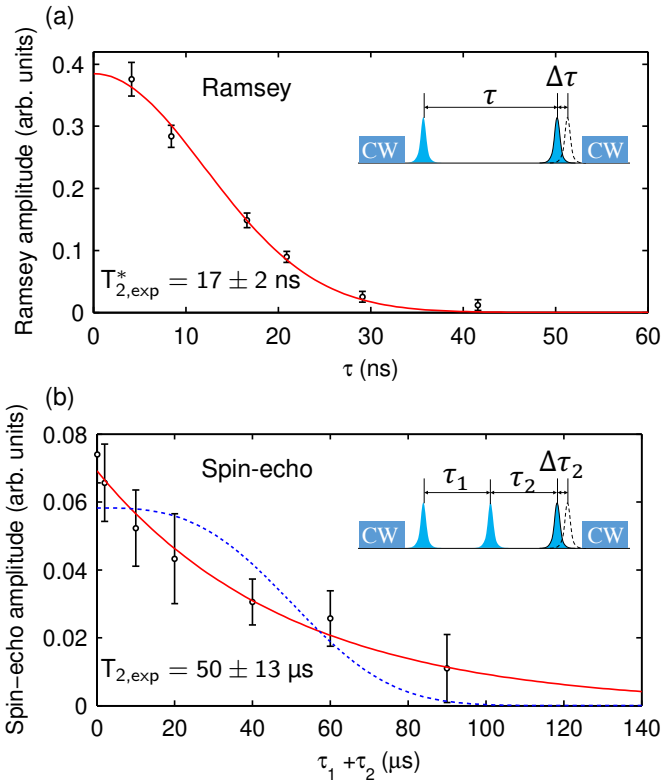

FIG. 4: (a) The Ramsey fringe amplitude as a function of delay time τ. The red curve shows a fit to $\exp(-(\tau/T_2^*)^2)$, giving $T_{2,\mathrm{exp}}^* = 17 \pm 2$ ns. (b) Spin-echo measurement of the dephasing time T_2. The delay $\tau_1 \simeq \tau_2$. Oscillations are observed by changing $\Delta\tau_2$. The oscillation amplitude is measured as a function of $\tau_1 + \tau_2$. The red curve shows a fit to $\exp(-\frac{\tau_1+\tau_2}{T_2})$, giving $T_{2,\mathrm{exp}} = 50 \pm 13$ μs. For comparison, the blue dashed line shows a fit to $\exp(-(\frac{\tau_1+\tau_2}{T_2})^3)$, the expected form for spectral diffusion. For these data, both the excitation and collection spot sizes are ∼0.6 μm. The temperature is at 5.5 K and the magnetic field is at 5 T. The ultra-fast pulses are detuned by $\Delta/2\pi = 0.9$ THz from the transition $|\downarrow\rangle \Leftrightarrow |\Downarrow\uparrow\downarrow\rangle$.

V. T_2^* AND T_2 MEASUREMENT

T_2^* is extracted from the decay of the Ramsey fringe amplitude as a function of the pulse delay time, as shown in Fig. 4(a). A fit for data in Fig. 4(a) using $\exp(-(\tau/T_2^*)^2)$ gives $T_{2,\mathrm{exp}}^* = 17 \pm 2$ ns, which is consistent with prior studies [51, 52]. This dephasing time originates from the inhomogeneous nuclear field due to the hyperfine interaction between electrons and lattice nuclear spins. For the Ga donors in ZnO, this includes the hyperfine interaction from both the Ga nucleus and the ^{67}Zn nuclei. T_2^* can be estimated from the dispersion of the hyperfine field Δ_B with $T_2^* = \hbar/g_e\mu_B\Delta_B$ [53]. As only one Ga nucleus is in the effective wave function of the electron bound to the donor, the effective field from Ga has 4 different values due to 3/2 nuclear spin of Ga:

$$B_{\mathrm{Ga}} = \frac{2\mu_0}{3g_e}\frac{\mu_{\mathrm{Ga}}}{I_{\mathrm{Ga}}}|u_{\mathrm{Zn}}|^2|\psi(0)|^2 \times \{\frac{3}{2}, \frac{1}{2}, -\frac{1}{2}, -\frac{3}{2}\}. \quad (3)$$

The hyperfine field due to numerous ^{67}Zn nuclei is estimated to have a Gaussian distribution $\exp(-B^2/\Delta_{B,\mathrm{Zn}}^2)$, where $\Delta_{B,\mathrm{Zn}}$ is calculated in Ref. [53]:

$$\Delta_{B,\mathrm{Zn}} = \frac{\mu_0\mu_{\mathrm{Zn}}}{g_e}\sqrt{\frac{32}{27}}\sqrt{\frac{I_{\mathrm{Zn}}+1}{I_{\mathrm{Zn}}}}|u_{\mathrm{Zn}}|^2\sqrt{f\sum_j|\psi(\vec{R}_j)|^4}, \quad (4)$$

In Eqs. 3 and 4, μ_B is the Bohr magneton, g_e is the electron g-factor, μ_0 is the vacuum permeability. $I_{\mathrm{Zn}} = 5/2$ ($I_{\mathrm{Ga}} = 3/2$) is the nuclear spin of ^{67}Zn (Ga), $\mu_{\mathrm{Zn}} = 0.874\mu_N$ ($\mu_{\mathrm{Ga}} = 2.24\mu_N$) is the nuclear magnetic moment of ^{67}Zn (Ga) and μ_N is the nuclear magneton. $f = 4.1\%$ is the natural abundance of ^{67}Zn. $\psi(\vec{R}_j)$ ($\psi(0)$) is the hydrogenic effective-mass envelope wave function of electron at the jth Zn (Ga) lattice site. $|u_{\mathrm{Zn}}|^2$ is the ratio of Bloch function density at the Zn site to the average Bloch function density. From electron spin resonance measurements in ZnO [33], $|u_{\mathrm{Zn}}|^2 \simeq 1120$. Using the effective mass Bohr radius $a_{\mathrm{B}} \simeq 1.7$ nm and by combining the hyperfine interactions from both Ga and ^{67}Zn, we find $T_{2,\mathrm{theory}}^* \simeq 9$ ns [42], which is on the same order as our experimental result. Moving to isolated single donors in isotope-purified ZnO can eliminate this dephasing mechanism.

We next apply a spin echo sequence to suppress the effect of the inhomogeneous nuclear field. A standard spin echo includes two $\pi/2$ pulses separated by one π pulse. It has been shown that three small angle rotations have a similar effect but with a smaller echo signal [25]. The measured spin-echo decoherence time is $T_{2,\mathrm{exp}} = 50 \pm 13$ μs using an exponential fit, as shown in Fig. 4(b). Possible mechanisms limiting T_2 are instantaneous diffusion and spectral diffusion.

Instantaneous diffusion (ID) is the decoherence caused by the refocusing pulse in the spin-echo sequence. During the refocusing pulse, the dipole-coupled electron spins bound to different donors all rotate with the same angle. Therefore, the energy of this dipole-dipole interaction doesn't flip sign after the refocusing pulse and the phase cannot be corrected. The decay of the signal follows an $\exp(-t/T_{2,\mathrm{ID}})$ with $T_{2,\mathrm{ID}}$ given by [54, 55]

$$1/T_{2,\mathrm{ID}} = \frac{\mu_0(g_e\mu_B)^2 N_{\mathrm{Ga}}}{9\sqrt{3}\pi\hbar}\sin^2\frac{\theta_2}{2} \quad (5)$$

where N_{Ga} is the density of Ga donors and θ_2 is the rotation angle of the refocusing pulse. Due to the comparable excitation and collection spot sizes in the experiment, the rotation angle varies across the collection spot making an accurate estimation of θ_2 challenging. A reasonable range of θ_2 is $\pi/5 \sim \pi/2$. While the Ga concentration is uncertain, ESR measurements of a similar substrate indicate a shallow donor concentration of $\simeq 10^{16}$ cm^{-3} [56]. Using this estimate, $T_{2,\mathrm{ID}}$ ranges from 240 μs to 1.27 ms. It is also possible that the refocusing pulse incoherently alters the local spin

environment due to charge transfer between deeper paramagnetic centers (e.g. Li) [56] causing additional dephasing.

Spectral diffusion (SD) of the electron spin energy can occur due to flip-flops of dipole-coupled ^{67}Zn nuclear spins. The measured $T_{2,exp}^{ZnO}$ is of similar magnitude to T_2 measured for phosphorous donors in natural Si [57, 58], which is limited by this spectral diffusion mechanism. Considering the similar isotope composition between ZnO and Si, we expect spectral diffusion to also be significant in ZnO. We estimate $T_{2,SD}$ with a stochastic model developed for phosphorous donors in Si [59]. Assuming a Gaussian diffusion kernel, the decay of the signal exhibits an $\exp(-(t/T_{2,SD})^3)$ dependence with $T_{2,SD}$ given by

$$1/T_{2,SD} \simeq \left[\frac{8\pi}{27\sqrt{3}\hbar}\mu_0\mu_{Zn}g_e\mu_B n\Sigma_j b_j^2\right]^{1/3}, \quad (6)$$

$$\Sigma_j b_j^2 = f\frac{\mu_0^2}{16\pi^2}\frac{\mu_{Zn}^4}{\hbar^2}\Sigma_j\frac{(1-3\cos^2\theta_j)^2}{r_j^6}, \quad (7)$$

where n is the density of ^{67}Zn. For a given ^{67}Zn nucleus, b_j is the dipole-dipole interaction between it and the jth ^{67}Zn. r_j is the distance between the two nuclei and θ_j is the angle between $\vec{r_j}$ and the B-field. Using Eq. 6, we estimate $T_{2,SD} \simeq 200$ µs.

The magnitude of T_2 estimated by both mechanisms is in reasonable agreement with $T_{2,exp}$. While we find better agreement in the experimental decay shape with the instantaneous diffusion mechanism, as shown in Fig. 4(b), it is still hard to confirm the dominant mechanism considering the low signal-to-noise ratio and since the dependence of T_2 on different parameters has not been measured. To rigorously determine the mechanism, future experiments will be conducted to measure the dependence of T_2 on the abundance of ^{67}Zn [60], donor density [38], rotation angle of the rephasing pulse [55] and magnetic field direction [57]. The determination of the mechanism is important as this can be generalized to other II-VI materials, thus aiding in the search for superior defect-based qubit candidates. Regardless of which mechanism dominates T_2 in ZnO, practical devices will require both isotope purification and lower donor densities.

VI. OUTLOOK

In summary, we demonstrate optical spin control and read-out of Ga donor qubits in a bulk ZnO crystal. Long spin relaxation times (100 ms) and coherence times (50 µs) are observed. These promising results motivate future work on the challenges toward making a practical quantum network out of optically-active donor qubits. In the ZnO donor platform, these challenges include chemical and isotope purification of the sample, high fidelity microwave control of the spin state, and single donor isolation. Thin films grown by molecular beam epitaxy have shown orders of magnitude lower impurity concentration than commercial ZnO substrates [39]. Devices incorporating such high-purity layers will be essential for addressing all three challenges. In the near-term, single donor isolation for fundamental studies can be achieved in nanostructures fabricated by focused ion beam milling [61] or utilizing single nanowires [62]. In the long term, scalable device integration will require pushing ZnO fabrication techniques beyond the standard microfabrication techniques currently developed for ZnO [32, 63].

VII. ACKNOWLEDGEMENTS

This material is based upon work supported by the National Science Foundation under Grant No. 1150647, and in part upon work supported by the State of Washington through the University of Washington Clean Energy Institute and via funding from the Washington Research Foundation. K.-M. C. Fu acknowledges the support from the Research Corporation for Science Advancement as a Cottrell Scholar. Y. K. acknowledges JST, PRESTO Grant Number JPMJPR1763, Japan. We acknowledge Kelsey Bates for the measurement of the laser pulse length. We acknowledge Atsushi Tsukazaki and Joseph Falson for useful discussions on ZnO growth, properties, and characterization.

[1] Khabat Heshami, Duncan G. England, Peter C. Humphreys, Philip J. Bustard, Victor M. Acosta, Joshua Nunn, and Benjamin J. Sussman, Quantum memories: emerging applications and recent advances, J. of Mod. Opt. **63**, 2005 (2016).

[2] Adeline Orieux and Eleni Diamanti, Recent advances on integrated quantum communications, Journal of Optics **18**, 083002 (2016).

[3] T. D. Ladd, F. Jelezko, R. Laflamme, Y. Nakamura, C. Monroe, and J. L. O'Brien, Quantum computers, Nature **464**, 45 (2010).

[4] Simon C. Benjamin, Brendon W. Lovett, and Jason M. Smith, Prospects for measurement-based quantum computing with solid state spins, Laser and Photonics Rev. **3**, 556 (2009).

[5] Naomi H. Nickerson, Ying Li, and Simon C. Benjamin, Topological quantum computing with a very noisy network and local error rates approaching one percent, Nat. Commun. **4**, 1756 (2013).

[6] Robert Raussendorf and Hans J. Briegel, A One-Way Quantum Computer, Phys. Rev. Lett. **86**, 5188 (2001).

[7] Nicolas Sangouard, Christoph Simon, Hugues de Riedmatten, and Nicolas Gisin, Quantum repeaters based on atomic ensembles and linear optics, Rev. of Mod. Phys. **83**, 33 (2011).

[8] H.-J. Briegel, W. Dür, J. I. Cirac, and P. Zoller, Quantum repeaters: The role of imperfect local operations in quantum communication, Phys. Rev. Lett. **81**, 5932 (1998).

[9] C. Santori, P. E. Barclay, K-M C. Fu, R. G. Beausoleil, S. Spillane, and M. Fisch, Nanophotonics for quantum optics using nitrogen-vacancy centers in diamond, Nanotech-

nology **21**, 274008 (2010).
[10] Marcus W. Doherty, Neil B. Manson, Paul Delaney, Fedor Jelezko, Jörg Wrachtrup, and Lloyd C. L. Hollenberg, The nitrogen-vacancy colour centre in diamond, Physics Reports **528**, 1 (2013).
[11] Peter C. Humphreys, Norbert Kalb, Jaco P. J. Morits, Raymond N. Schouten, Raymond F. L. Vermeulen, Daniel J. Twitchen, Matthew Markham, and Ronald Hanson, Deterministic delivery of remote entanglement on a quantum network, Nature **558**, 268 (2018).
[12] Tim Schröder, Sara L. Mouradian, Jiabao Zheng, Matthew E. Trusheim, Michael Walsh, Edward H. Chen, Luozhou Li, Igal Bayn, and Dirk Englund, Quantum nanophotonics in diamond, J. Opt. Soc. Am. B **33**, B65–B83 (2016).
[13] Roland Nagy, Matthias Widmann, Matthias Niethammer, Durga B. . R. Dasari, Ilja Gerhardt, Öney O. Soykal, Marina Radulaski, Takeshi Ohshima, Jelena Vučković, Nguyen T. Son, Ivan G. Ivanov, Sophia E. Economou, Cristian Bonato, Sang-Yun Lee, and Jörg Wrachtrup, Quantum Properties of Dichroic Silicon Vacancies in Silicon Carbide, Phys. Rev. Applied **9**, 034022 (2018).
[14] David J. Christle, Paul V. Klimov, Charles F. de las Casas, Krisztián Szász, Viktor Ivády, Valdas Jokubavicius, Jawad Ul Hassan, Mikael Syväjärvi, William F. Koehl, Takeshi Ohshima, Nguyen T. Son, Erik Janzén, Ádám Gali, and David D. Awschalom, Isolated Spin Qubits in SiC with a High-Fidelity Infrared Spin-to-Photon Interface, Phys. Rev. X **7**, 021046 (2017).
[15] Kamyar Saeedi, Stephanie Simmons, Jeff Z. Salvail, Phillip Dluhy, Helge Riemann, Nikolai V. Abrosimov, Peter Becker, Hans-Joachim Pohl, John J. L. Morton, and Mike L. W. Thewalt, Room-temperature quantum bit storage exceeding 39 minutes using ionized donors in silicon-28, Science **342**, 830 (2013).
[16] Thomas F. Watson, Bent Weber, Yu-Ling Hsueh, Lloyd C. L. Hollenberg, Rajib Rahman, and Michelle Y. Simmons, Atomically engineered electron spin lifetimes of 30 s in silicon, Sci. Adv. **3**, e1602811 (2017).
[17] J. T. Muhonen, A. Laucht, S. Simmons, J. P. Dehollain, R. Kalra, F. E. Hudson, S. Freer, K. M. Itoh, D. N. Jamieson, J. C. McCallum, A. S. Dzurak, and A. Morello, Quantifying the quantum gate fidelity of single-atom spin qubits in silicon by randomized benchmarking, J. Phys.: Condens. Matter **27**, 154205 (2015).
[18] Naomi H. Nickerson, Joseph F. Fitzsimons, and Simon C. Benjamin, Freely scalable quantum technologies using cells of 5-to-50 qubits with very lossy and noisy photonic links, Phys. Rev. X **4**, 041041 (2014).
[19] Guilherme Tosi, Fahd A. Mohiyaddin, Vivien Schmitt, Stefanie Tenberg, Rajib Rahman, Gerhard Klimeck, and Andrea Morello, Silicon quantum processor with robust long-distance qubit couplings, Nat. Commun. **8**, 450 (2017).
[20] I. Izeddin, M. A. J. Klik, N. Q. Vinh, M. S. Bresler, and T. Gregorkiewicz, Donor-State-Enabling Er-Related Luminescence in Silicon: Direct Identification and Resonant Excitation, Phys. Rev. Lett. **99**, 077401 (2007).
[21] Kevin J. Morse, Rohan J. S. Abraham, Adam DeAbreu, Camille Bowness, Timothy S. Richards, Helge Riemann, Nikolay V. Abrosimov, Peter Becker, Hans-Joachim Pohl, Michael L. W. Thewalt, and Stephanie Simmons, A photonic platform for donor spin qubits in silicon, Sci. Adv. **3**, e1700930 (2017).
[22] C. Beaufils, W. Redjem, E. Rousseau, V. Jacques, Kuznetsov, C. Raynaud, C. Voisin, A. Benali, T. Herzig, S. Pezzagna, J. Meijer, M. Abbarchi, and G. Cassabois, Optical properties of an ensemble of G-centers in silicon, Phys. Rev. B **97**, 035303 (2018).
[23] Kai-Mei C. Fu, Wenzheng Yeo, Susan Clark, Charles Santori, Colin Stanley, M. C. Holland, and Yoshihisa Yamamoto, Millisecond spin-flip times of donor-bound electrons in GaAs, Phys. Rev. B **74**, 121304 (2006).
[24] Kai-Mei C. Fu, Susan M. Clark, Charles Santori, Colin R. Stanley, M. C. Holland, and Yoshihisa Yamamoto, Ultrafast control of donor-bound electron spins with single detuned optical pulses, Nature Physics **4**, 780 (2008).
[25] Susan M. Clark, Kai-Mei C. Fu, Qiang Zhang, Thaddeus D. Ladd, Colin Stanley, and Yoshihisa Yamamoto, Ultrafast Optical Spin Echo for Electron Spins in Semiconductors, Phys. Rev. Lett. **102**, 247601 (2009).
[26] David Press, Thaddeus D. Ladd, Bingyang Zhang, and Yoshihisa Yamamoto, Complete quantum control of a single quantum dot spin using ultrafast optical pulses, Nature **456**, 218 (2008).
[27] Miro Kroutvar, Yann Ducommun, Dominik Heiss, Max Bichler, Dieter Schuh, Gerhard Abstreiter, and Jonathan J. Finley, Optically programmable electron spin memory using semiconductor quantum dots, Nature **432**, 81 (2004).
[28] Aymeric Delteil, Zhe Sun, Wei-bo Gao, Emre Togan, Stefan Faelt, and Ataç Imamoğlu, Generation of heralded entanglement between distant hole spins, Nature Physics **12**, 218 (2015).
[29] Kai-Mei C. Fu, Charles Santori, Colin Stanley, M. C. Holland, and Yoshihisa Yamamoto, Coherent population trapping of electron spins in a high-purity n-type gaas semiconductor, Phys. Rev. Lett. **95**, 187405 (2005).
[30] M. R. Wagner, G. Callsen, J. S. Reparaz, J.-H. Schulze, R. Kirste, M. Cobet, I. A. Ostapenko, S. Rodt, C. Nenstiel, M. Kaiser, A. Hoffmann, A. V. Rodina, M. R. Phillips, S. Lautenschläger, S. Eisermann, and B. K. Meyer, Bound excitons in zno: Structural defect complexes versus shallow impurity centers, Phys. Rev. B **84**, 035313 (2011).
[31] U. Ozgur, Ya. I. Alivov, C. Liu, A. Teke, M. A. Reshchikov, S. Dogan, V. Avrutin, S.-J. Cho, and H. Morkoc, A comprehensive review of zno materials and devices, Journal of Applied Physics **98**, 041301 (2005).
[32] A. B. Djurišić, A. M.C. Ng, and X. Y. Chen, ZnO nanostructures for optoelectronics: Material properties and device applications, Prog. Quantum Electron. **34**, 191 (2010).
[33] C. Gonzalez, D. Block, R.T. Cox, and A. Herve, Magnetic resonance studies of shallow donors in zinc oxide, J. Cryst. Growth **59**, 357 (1982).
[34] M. Steger, K. Saeedi, M. L. W. Thewalt, J. J. L. Morton, H. Riemann, N. V. Abrosimov, P. Becker, and Pohl, Quantum Information Storage for over 180 s Using Donor Spins in a 28Si "Semiconductor Vacuum", Science **336**, 1280 (2012).
[35] Lucio Robledo, Lilian Childress, Hannes Bernien, Bas Hensen, Paul F. A. Alkemade, and Ronald Hanson, High-fidelity projective read-out of a solid-state spin quantum register, Nature **477**, 574 (2011).
[36] S. C. Benjamin, D. E. Browne, J. Fitzsimons, and J. J. L. Morton, Brokered graph-state quantum computation, New J. of Phys. **8**, 141 (2006).
[37] Rogerio de Sousa and S. Das Sarma, Theory of nuclear-induced spectral diffusion: Spin decoherence of phosphorus donors in Si and GaAs quantum dots, Phys. Rev. B **68**, 115322 (2003).
[38] Alexei M. Tyryshkin, Shinichi Tojo, John J. L. Morton, Helge Riemann, Nikolai V. Abrosimov, Peter Becker, Hans-Joachim Pohl, Thomas Schenkel, Michael L. W. Thewalt, Kohei M. Itoh, and S. A. Lyon, Electron spin coherence

exceeding seconds in high-purity silicon, Nature Mater. **11**, 143 (2011).
[39] Shunsuke Akasaka, Ken Nakahara, Atsushi Tsukazaki, Akira Ohtomo, and Masashi Kawasaki, $Mg_xzn_{1-x}o$ films with a low residual donor concentration ($< 10^{15} cm^{-3}$) grown by molecular beam epitaxy, Appl. Phys. Express **3**, 071101 (2010).
[40] M. Nakano, A. Tsukazaki, R. Y. Gunji, K. Ueno, A. Ohtomo, T. Fukumura, and M. Kawasaki, Schottky contact on a ZnO (0001) single crystal with conducting polymer, App. Phys. Lett. **91**, 142113 (2007).
[41] B. K. Meyer, H. Alves, D. M. Hofmann, W. Kriegseis, D. Forster, F. Bertram, J. Christen, A. Hoffmann, M. Straßburg, M. Dworzak, U. Haboeck, and A. V. Rodina, Bound exciton and donoracceptor pair recombinations in ZnO, Phys. Status Solidi B **241**, 231 (2004).
[42] See supplementary information for details on sample description, line identification of spectra, selection rule, calibration of spin population, determination of polarization, detail of the fit using the 4-level density matrix method, and the estimation of the inhomogeneous hyperfine field distribution.
[43] Markus R. Wagner, Jan-Hindrik Schulze, Ronny Kirste, Munise Cobet, Axel Hoffmann, Christian Rauch, Anna V. Rodina, Bruno K. Meyer, Uwe Röder, and Klaus Thonke, $Gamma_7$ valence band symmetry related hole fine splitting of bound excitons in zno observed in magneto-optical studies, Phys. Rev. B **80**, 205203 (2009).
[44] C. Cabrillo, J. I. Cirac, P. García-Fernández, and P. Zoller, Creation of entangled states of distant atoms by interference, Phys. Rev. A **59**, 1025 (1999).
[45] Jungtaek Kim, J. Puls, S. Sadofev, and F. Henneberger, Charged carrier spin dynamics in ZnO quantum wells and epilayers, Phys. Rev. B **93**, 045306 (2016).
[46] S. V. Poltavtsev, A. N. Kosarev, I. A. Akimov, D. R. Yakovlev, S. Sadofev, J. Puls, S. P. Hoffmann, M. Albert, C. Meier, T. Meier, and M. Bayer, Time-resolved photon echoes from donor-bound excitons in ZnO epitaxial layers, Phys. Rev. B **96**, 035203 (2017).
[47] Xiayu Linpeng, Todd Karin, M. V. Durnev, Russell Barbour, M. M. Glazov, Sherman, S. P. Watkins, Satoru Seto, and Kai-Mei C. Fu, Longitudinal spin relaxation of donor-bound electrons in direct band-gap semiconductors, Phys. Rev. B **94**, 125401 (2016).
[48] Alexander V. Khaetskii and Yuli V. Nazarov, Spin-flip transitions between Zeeman sublevels in semiconductor quantum dots, Phys. Rev. B **64**, 125316 (2001).
[49] Susan M. Clark, Kai-Mei C. Fu, Thaddeus D. Ladd, and Yoshihisa Yamamoto, Quantum Computers Based on Electron Spins Controlled by Ultrafast Off-Resonant Single Optical Pulses, Phys. Rev. Lett. **99**, 040501 (2007).
[50] S. E. Harris, Refractive-index control with strong fields, Opt. Lett. **19**, 2018 (1994).
[51] H. Horn, A. Balocchi, X. Marie, A. Bakin, A. Waag, M. Oestreich, and J. Hübner, Spin noise spectroscopy of donor-bound electrons in ZnO, Phys. Rev. B **87**, 045312 (2013).
[52] Sebastian Kuhlen, Ralph Ledesch, Robin de Winter, Matthias Althammer, Sebastian T. B. Gönnenwein, Matthias Opel, Rudolf Gross, Thomas A. Wassner, Martin S. Brandt, and Bernd Beschoten, Unambiguous determination of spin dephasing times in ZnO by time-resolved magneto-optical pump-probe experiments, Phys. Status Solidi B **251**, 1861 (2014).
[53] I. A. Merkulov, Al Efros, and M. Rosen, Electron spin relaxation by nuclei in semiconductor quantum dots, Phys. Rev. B **65**, 205309 (2002).
[54] Vadim V. Kurshev and Tsuneki Ichikawa, Effect of spin flip-flop on electron-spin-echo decay due to instantaneous diffusion, J. Magn. Reson. **96**, 563 (1992).
[55] J. Tribollet, J. Behrends, and K. Lips, Ultra long spin coherence time for Fe 3+ in ZnO: A new spin qubit, Europhys. Lett. **84**, 20009 (2008).
[56] Yongquan Jiang, N. C. Giles, and L. E. Halliburton, Persistent photoinduced changes in charge states of transition-metal donors in hydrothermally grown ZnO crystals, J.of Appl. Phys. **101**, 093706 (2007).
[57] A. M. Tyryshkin, J. J. L. Morton, S. C. Benjamin, A. Ardavan, G. A. D. Briggs, J. W. Ager, and S. A. Lyon, Coherence of spin qubits in silicon, J. Phys. Condens. Matter **18**, 783 (2006).
[58] W. M. Witzel and S. Das Sarma, Quantum theory for electron spin decoherence induced by nuclear spin dynamics in semiconductor quantum computer architectures: Spectral diffusion of localized electron spins in the nuclear solid-state environment, Phys. Rev. B **74**, 035322 (2006).
[59] Meiro Chiba and Akira Hirai, Electron Spin Echo Decay Behaviours of Phosphorus Doped Silicon, J. the Phys. Soc. Jpn. **33**, 730 (1972).
[60] Kelly M. Whitaker, Stefan T. Ochsenbein, Alyssa L. Smith, Dorothy C. Echodu, Bruce H. Robinson, and Daniel R. Gamelin, Hyperfine Coupling in Colloidal n-Type ZnO Quantum Dots: Effects on Electron Spin Relaxation, J. Phys. Chem. C **114**, 14467 (2010).
[61] X. Wu, A. Yamilov, X. Liu, S. Li, V. P. Dravid, R. P. H. Chang, and H. Cao, Ultraviolet photonic crystal laser, Appl. Phys. Lett. **85**, 3657 (2004).
[62] Justin C. Johnson, Haoquan Yan, Peidong Yang, and Richard J. Saykally, Optical Cavity Effects in ZnO Nanowire Lasers and Waveguides, J. Phys. Chem. B **107**, 8816 (2003).
[63] S. J. Pearton, D. P. Norton, K. Ip, Y. W. Heo, and T. Steiner, Recent advances in processing of ZnO, J. Vac. Sci. Technol. B **22**, 932 (2004).